When Chiral Photons Meet Chiral Fermions: Photoinduced Anomalous Hall Effects in Weyl Semimetals

Ching-Kit Chan,[1] Patrick A. Lee,[1] Kenneth S. Burch,[2] Jung Hoon Han,[3,*] and Ying Ran[2,†]
[1]*Department of Physics, Massachusetts Institute of Technology, Cambridge, Massachusetts 02139, USA*
[2]*Department of Physics, Boston College, Chestnut Hill, Massachusetts 02467, USA*
[3]*Department of Physics, Sungkyunkwan University, Suwon 440-746, Korea*

(Received 27 September 2015; revised manuscript received 17 November 2015; published 15 January 2016)

The Weyl semimetal is characterized by three-dimensional linear band touching points called Weyl nodes. These nodes come in pairs with opposite chiralities. We show that the coupling of circularly polarized photons with these chiral electrons generates a Hall conductivity without any applied magnetic field in the plane orthogonal to the light propagation. This phenomenon comes about because with all three Pauli matrices exhausted to form the three-dimensional linear dispersion, the Weyl nodes cannot be gapped. Rather, the net influence of chiral photons is to shift the positions of the Weyl nodes. Interestingly, the momentum shift is tightly correlated with the chirality of the node to produce a net anomalous Hall signal. Application of our proposal to the recently discovered TaAs family of Weyl semimetals leads to an order-of-magnitude estimate of the photoinduced Hall conductivity which is within the experimentally accessible range.

DOI: 10.1103/PhysRevLett.116.026805

Introduction.—Previously thought to be an asset exclusive to massless elementary particles such as photons, chirality has now become a defining emergent property of electrons in such crystalline materials like graphene [1] and the surface of topological insulators [2]. An exciting new addition to the growing list of "chiral electronic materials" is the Weyl semimetal [3–7]. In this three-dimensional analogue of graphene, the Weyl nodes act as magnetic monopoles in momentum space [8]. In sharp contrast to the two Dirac nodes in graphene that behave more or less as separate low-energy degrees of freedom, a pair of Weyl nodes carrying opposite chiralities are inherently tied together in a nonlocal manner through the "chiral anomaly" mechanism which allows the dissipationless transfer of charge between them [9]. The subject has undergone vigorous research lately due to reports of material predictions, followed immediately by their synthesis and confirmation of their Weyl characters by photoemission experiments and nonlocal transport measurements. A striking example of success along this line in recent years is the transition metal monophosphide family that includes TaAs, TaP, NbAs, and NbP [10–19].

In light of the rapid maturity of the Weyl semimetal research, one should ask whether the unusual electronic transport properties in both the static and dynamic regimes of the Weyl semimetal can be exploited in high speed electronics or to provide a new means of revealing dynamic topological effects [18–20]. It was recently suggested that exposing a two-dimensional Dirac material to a circularly polarized (*CP*) light could lead to a novel form of Hall effect due to the effective gap opening at the Dirac point [21,22]. A natural question arises as to what happens when the three-dimensional, linearly dispersing bands of electrons couple to an intense *CP* light, as schematically presented in Fig. 1, and whether a nontrivial Hall effect can be induced. Here we present a direct consequence of coupling *CP* light to the Weyl fermion: the appearance of the anomalous Hall effect (AHE).

In this work, we show that even when the AHE is absent due to symmetry reasons in typical Weyl materials, it must be generally present in all Weyl systems when coupled to a *CP* light source. Based on a low-energy effective Weyl-Floquet Hamiltonian analysis and symmetry considerations, we discuss the induced AHE as a generic and readily

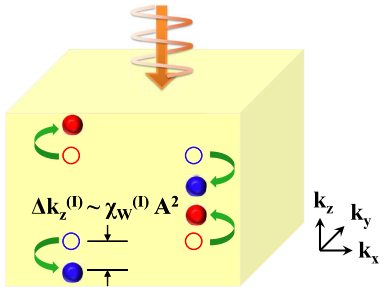

FIG. 1. Schematic figure for a driven Weyl semimetal. Blue and red circles indicate Weyl nodes with opposite chiralities $\chi_W^{(I)}$. The node positions are shifted by the chiral photons in a chirality-dependent manner and the shift is proportional to the square of the driving amplitude A. As a result, even though the total momentum shift along the driving direction is zero ($\sum_I \Delta k_z^{(I)} = 0$), the overall Chern vector shift has a finite z-component ($\delta\nu_z = \sum_I \chi_W^{(I)} \Delta k_z^{(I)} \neq 0$), resulting in a photoinduced anomalous Hall conductivity σ_{xy} [see Eq. (6)].

observable phenomenon in Weyl semimetals. We further demonstrate this effect using a concrete microscopic model, and apply our study to the TaAs family of Weyl semimetals with an estimation of the experimental feasibility. Other interesting works have addressed the driven three-dimensional Dirac electrons [23,24] or gapped systems [25,26]. However, neither systems enjoy the unique topological protection of the Weyl nodes, whose response, under a *CP* beam, results in the experimental signature of the AHE as we explain below.

General tight-binding model analysis.—The low-energy Hamiltonian for a single Weyl node can be parameterized most generally by a real 3-vector $\vec{\alpha}$ and a 3×3 real matrix β:

$$H_W(\vec{q}) = q_i\alpha_i\sigma_0 + q_i\beta_{ij}\sigma_j, \tag{1}$$

with a canonical 3D linear dispersion $E_W(\vec{q}) = \alpha_i q_i \pm [\sum_j(\sum_i q_i\beta_{ij})^2]^{1/2}$. Einstein summation is assumed in the momentum q_i and the Pauli matrix σ_j. The chirality of the Weyl node is given by the sign of the determinant of β: $\chi_W = \mathrm{sgn}[\mathrm{Det}(\beta)]$. For a practical band structure, this 2×2 Weyl Hamiltonian is embedded within a large N-band Hamiltonian as a low-energy sector. In order to have the most general consideration of the photoinduced AHE, we therefore consider an N-band tight-binding Hamiltonian $H(\vec{k})$. The expansion of $H(\vec{k})$ around a Weyl node at $\vec{k}_W$ to first order in $\vec{q} = \vec{k} - \vec{k}_W$ can be put in the block form:

$$U^\dagger H(\vec{k}_W + \vec{q})U = H_{\mathrm{lin}}(\vec{q}) + O(q^2),$$
$$H_{\mathrm{lin}}(\vec{q}) = \begin{pmatrix} H_{\mathrm{W}}(\vec{q}) & q_i C_i \\ q_i C_i^\dagger & D_0 + q_i D_i \end{pmatrix}, \tag{2}$$

where the matrix D_0 gives the $(N-2)$ high-energy states at $\vec{k} = \vec{k}_W$. Eigenvectors at $\vec{k} = \vec{k}_W$ are used to construct the unitary matrix U whose first two columns correspond to the two zero-energy states. In general, the $2\times(N-2)$ matrices C_i mix the Weyl bands with high-energy bands linearly in $\vec{q}$ and should not be ignored.

Without loss of generality, we consider an incident electromagnetic wave in the z direction with the vector potential $\vec{A}(t) = (A_x\cos(\omega t), A_y\sin(\omega t+\phi), 0)$. Following standard routes [21], the Peierls substitution $H_{\mathrm{lin}}(\vec{q}) \to H_{\mathrm{lin}}(\vec{q} + e\vec{A}(t))$ and averaging over one drive cycle leads to the effective Hamiltonian [27]:

$$H_{\mathrm{eff}}(\vec{q}) = \begin{pmatrix} H_{\mathrm{WF}}(\vec{q}) & O(q)+O(A^2) \\ O(q)+O(A^2) & D_0 + O(q) + O(A^2) \end{pmatrix}, \tag{3}$$

where the 2×2 Weyl-Floquet part reads

$$H_{\mathrm{WF}}(\vec{q}) = H_{\mathrm{W}}(\vec{q}) - \frac{e^2A_xA_y\cos\phi}{\omega} \times \left[\epsilon_{ijk}\beta_{xi}\beta_{yj}\sigma_k - \frac{i}{2}(C_xC_y^\dagger - C_yC_x^\dagger)\right]. \tag{4}$$

Higher-order terms $O(q^2) + O(qA^2) + O(A^4)$ are ignored. Clearly, the photoinduced effect is maximized for a *CP* light when $\cos\phi = \pm 1$, and vanishes for a linearly polarized beam.

The *CP* light has two contributions to the Weyl-Floquet Hamiltonian in Eq. (4). The first (β^2) term originates entirely from the two-band Weyl Hamiltonian $H_{\mathrm{W}}(\vec{q})$, while the second term proportional to $C_xC_y^\dagger - C_yC_x^\dagger$ is due to high-energy band mixing and must be kept in the construction of a general Weyl-Floquet effective model. For later convenience, we reparameterize $-(i/2)(C_xC_y^\dagger - C_yC_x^\dagger) = \kappa_0\sigma_0 + \kappa_i\sigma_i$ with four real numbers $\kappa_i = (-i/4)\mathrm{Tr}[\sigma_i(C_xC_y^\dagger - C_yC_x^\dagger)]$. Therefore, the influence of the drive to A^2 order on the 2×2 Weyl band can be summarized as

$$H_{\mathrm{WF}}(\vec{q}) = (q_i - \delta q_i)\alpha_i\sigma_0 + (q_i - \delta q_i)\beta_{ij}\sigma_j - \delta\mu\cdot\sigma_0,$$
$$\delta q_i = \frac{e^2A_xA_y\cos\phi}{\omega}[\epsilon_{jkl}\beta_{xj}\beta_{yk} + \kappa_l](\beta^{-1})_{li},$$
$$\delta\mu = -\delta\vec{q}\cdot\vec{\alpha} + \frac{e^2A_xA_y\cos\phi}{\omega}\kappa_0. \tag{5}$$

δq_i and $\delta\mu$ represent the shifts of Weyl momenta and chemical potential, respectively.

The photoinduced Weyl node shift has an immediate consequence on the electronic transport. According to Ref. [6], for a Weyl system where the chemical potential situates at the nodes (i.e., $\mu = 0$), the leading order change of the anomalous Hall conductivity is governed by the momentum shifts of every Weyl node as

$$\delta\sigma_{ij} = \frac{e^2}{2\pi h}\epsilon_{ijk}\delta\nu_k, \quad \text{where } \delta\nu_k = \sum_I \chi_W^{(I)}\cdot\delta q_k^{(I)}. \tag{6}$$

Different Weyl nodes are labeled by the superscript I and $\delta\vec{\nu}$ is the change of the Chern vector [6]. Provided that the momentum shifts $\delta q_k^{(I)}$ among Weyl nodes of different chiralities $\chi_W^{(I)}$ do not cancel out, one would expect the AHE induced at the A^2 order to be proportional to the intensity of the incident beam. Note that the photoinduced self-doping ($\delta\mu \neq 0$) of the Weyl nodes contributes to $\delta\sigma_{ij}$ at a higher order $O(\delta\mu^2) = O(A^4)$ [6] of the drive intensity, which is negligible. If $\vec{\kappa}^{(I)} = 0$, one can show the z-component of the Chern vector shift to be

$$\delta\nu_z = \frac{e^2A_xA_y\cos\phi}{\omega}\sum_{I,i}\frac{[\mathrm{Cof}(\beta^{(I)})_{zi}]^2}{|\det(\beta^{(I)})|}, \tag{7}$$

where $\mathrm{Cof}(\beta^{(I)})_{ij}$ is the ij element of the cofactor matrix of $\beta^{(I)}$. The alternating signs of $\chi^{(I)}$ between a node and an antinode, or a monopole and an antimonopole, are precisely cancelled by the same sign change in $\delta q_z^{(I)}$. As such, each Weyl node has a positive-definite contribution to $\delta\nu_z$. Consequently, a finite Hall conductivity is induced in the plane perpendicular to the incident beam and its sign is determined by the photon chirality through $\sigma_{xy} \propto \cos\phi$.

In practice, the pre-drive chemical potential μ may not cross the Weyl node as we have discussed so far. As long as μ before the drive lies in the linearly dispersive regime near the node, one can show that the our resultant $\delta\sigma_{ij}$ is unaffected [27]. In fact, using a frequency of excitation $0 < \omega < 2\mu$ for slightly electron-doped Weyl node would ensure no absorption, as assumed here, and thus should lead to a more straightforward analysis of the experimental results regarding the photoinduced AHE.

Symmetry consideration for multiple Weyl nodes.—In a typical Weyl material, there are multiple sets of Weyl nodes related by the space group and time-reversal (TR) symmetries [5,10]. The parameters $\vec{\alpha}$, β, and C_i characterizing symmetry-related nodes transform accordingly. We now derive their transformation rules and discuss how the nodal shifts $\delta\vec{q}$ and $\delta\mu$ among the symmetry-related nodes are correlated.

A pair of Weyl points $\vec{k}_W^{(I)}$ (with $I = 1, 2$) related by some space-group symmetry satisfy $R\vec{k}_W^{(1)} = \vec{k}_W^{(2)}$, where $R \in O(3)$ defines the particular symmetry operation. The parameters quantifying the Weyl nodes transform according to

$$\alpha_i^{(2)} = R_{ij}\alpha_j^{(1)}, \quad \beta_{ij}^{(2)} = R_{ik}\beta_{kj}^{(1)}, \quad C_i^{(2)} = R_{ij}C_j^{(1)}. \quad (8)$$

As a result, the chiralities of nodes related by a rotation ($\mathrm{Det}[R] = +1$) are the same, whereas a mirror or inversion operation ($\mathrm{Det}[R] = -1$) produces a sign difference. On the other hand, nodes related by an anti-unitary symmetry involving TR operation satisfy

$$\alpha_i^{(2)} = R_{ij}\alpha_j^{(1)}, \quad \beta_{ij}^{(2)} = R_{ik}\beta_{kl}^{(1)}\xi_{lj}, \quad C_i^{(2)} = R_{ij}[C_j^{(1)}]^*. \quad (9)$$

Because of the presence of $\xi = (\xi_{lj}) = \mathrm{diag}(1, -1, 1)$, the chiralities of these two nodes are related by $-\mathrm{Det}[R]$. For instance, the TR operation with $R = \mathrm{diag}(-1, -1, -1)$ gives the same chirality for the nodes at $\vec{k}_W$ and $R\vec{k}_W = -\vec{k}_W$.

Some proposed Weyl semimetals break TR symmetry but preserve inversion (I). Our symmetry analysis predicts $\vec{\alpha}^{(2)} = -\vec{\alpha}^{(1)}$, $\beta^{(2)} = -\beta^{(1)}$, $\kappa_0^{(2)} = \kappa_0^{(1)}$ and $\vec{\kappa}^{(2)} = \vec{\kappa}^{(1)}$ for a pair of I-related nodes and thus, using Eq. (5),

$$\delta\vec{q}^{(2)} = -\delta\vec{q}^{(1)}, \qquad \delta\mu^{(2)} = \delta\mu^{(1)}(I\text{-related}). \quad (10)$$

Since these two nodes must have opposite chiralities ($\mathrm{Det}[R] = -1$), the product $\chi^{(I)}\delta\vec{q}^{(I)}$ is identical for both of them. Hence, from Eq. (6), these two nodes contribute additively to the Hall conductivity. A similar conclusion holds for I symmetry breaking Weyl materials for which TR is a good symmetry. In this case we find $\vec{\alpha}^{(2)} = -\vec{\alpha}^{(1)}$, $\beta^{(2)} = -\beta^{(1)} \cdot \xi$, $\kappa_0^{(2)} = -\kappa_0^{(1)}$ and $\vec{\kappa}^{(2)} = -\xi \cdot \vec{\kappa}^{(1)}$ for TR-related nodes, and thus

$$\delta\vec{q}^{(2)} = \delta\vec{q}^{(1)}, \qquad \delta\mu^{(2)} = -\delta\mu^{(1)}(\text{TR-related}). \quad (11)$$

Since $\chi^{(1)} = \chi^{(2)}$, Eq. (6) once again predicts constructive contributions from the TR-related nodes.

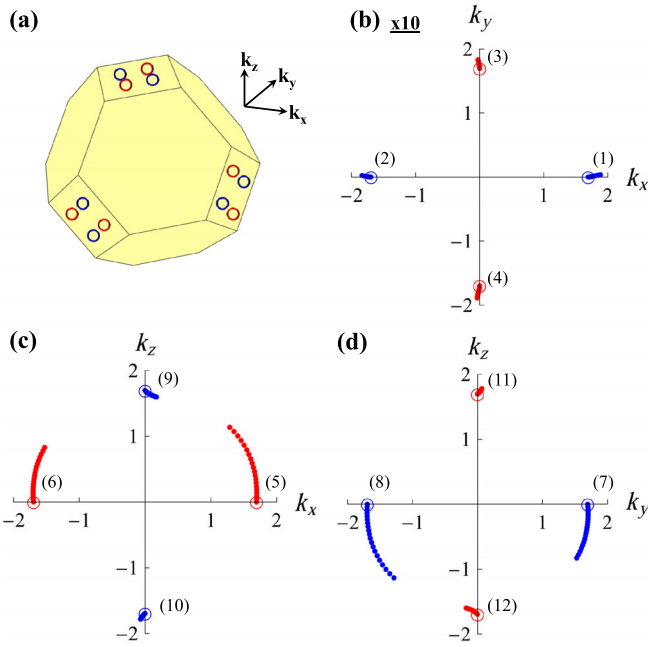

FIG. 2. (a) The 12 Weyl nodes in the first Brillouin zone of the undriven lattice Weyl model studied in Ref. [30]. (b), (c), and (d) Photoinduced Weyl node shifts in the presence of a CP drive along the z direction. Nodes with positive (negative) chirality are represented by red (blue) dots, and (I) labels the I-th Weyl node [see Eq. (12)]. Open circles denote the undriven Weyl node positions. Only projections on the $k_z = 2\pi$, $k_y = 2\pi$, and $k_x = 2\pi$ planes are shown as we increase A^2 from 0 to 0.3. The shifts in (b) are magnified 10 times for a better visualization. Details of the model calculation can be found in Ref. [27]. Parameters used: $(t, \epsilon, \lambda, \omega) = (1, 3, 1, 1.1)$.

Lattice model analysis.—To illustrate our findings, we now proceed to study a concrete lattice model for a Weyl semimetal of the inversion symmetry breaking type [30]. The model is parameterized by the hopping (t), spin-orbit coupling (λ), and inversion breaking potential (ϵ) [27]. The bare system possesses 12 Weyl nodes labeled as [see Fig. 2(a)]:

$$\begin{aligned} \vec{k}_{W-}^{(1,2)} &= (\pm k_0, 0, 2\pi), & \vec{k}_{W+}^{(3,4)} &= (0, \pm k_0, 2\pi), \\ \vec{k}_{W+}^{(5,6)} &= (\pm k_0, 2\pi, 0), & \vec{k}_{W-}^{(7,8)} &= (2\pi, \pm k_0, 0), \\ \vec{k}_{W-}^{(9,10)} &= (0, 2\pi, \pm k_0), & \vec{k}_{W+}^{(11,12)} &= (2\pi, 0, \pm k_0), \end{aligned} \quad (12)$$

along with their chiralities as subscripts $\pm$ and a characteristic momentum $k_0 = 2\sin^{-1}[\epsilon/(4\lambda)]$. In the presence of a CP drive, each node undergoes a momentum shift given by

$$-\delta\vec{q}_{-}^{(1,2)} = \delta\vec{q}_{+}^{(3,4)} = \frac{e^2A^2}{\omega}\frac{8\eta(1-\eta)\lambda^2}{\epsilon}\hat{z},$$
$$\delta\vec{q}_{+}^{(5,6)} = -\delta\vec{q}_{-}^{(7,8)} = \frac{e^2A^2}{\omega}\frac{8\eta(1+\eta)\lambda^2}{\epsilon}\hat{z},$$
$$-\delta\vec{q}_{-}^{(9,10)} = \delta\vec{q}_{+}^{(11,12)} = \frac{e^2A^2}{\omega}\frac{\epsilon t^2}{16\eta\lambda^2}\hat{z}, \quad (13)$$

with $\eta = \sqrt{1-\epsilon^2/16\lambda^2}$. The momentum shifts clearly correlate with the chiralities. The photoinduced self-dopings are

$$-\delta\mu^{(9)} = \delta\mu^{(10)} = \delta\mu^{(11)} = -\delta\mu^{(12)} = \frac{e^2A^2}{\omega}\frac{\epsilon^2}{16}, \quad (14)$$

and $\delta\mu^{(1-8)} = 0$. The anomalous Hall conductivity obtained is (up to A^2 order):

$$\delta\sigma_{xy} = \frac{e^2}{2\pi h}\frac{e^2A^2}{\omega}\left(\frac{64\eta\lambda^2}{\epsilon} + \frac{\epsilon t^2}{4\eta\lambda^2}\right), \quad (15)$$

which agrees with the expectation of the low-energy analysis.

So far all our discussion have been done within the effective Hamiltonian scheme valid for a small driving amplitude. A more stringent check free from this assumption is offered by solving the full Floquet Hamiltonian whose matrix elements are $\langle n'|H_F|n\rangle = H_{n-n'} + n\omega\delta_{n,n'}I_4$ with $n(n')$ denoting the $n(n')$-th Floquet band. The topological character of the Weyl nodes indeed protects them against the drive, and only their locations are shifted continuously in a chirality-dependent way. Figure 2(b)–(d) demonstrate the Weyl node shifts obtained from diagonalizing the full Floquet Hamiltonian as we increase the driving field strength. It is obvious that nodes with opposite chirality have opposite shifts in k_z, leading to an imbalance of $\delta\nu_z$ and eventually, a net anomalous Hall conductivity. The overall field dependence of the sum of Δk_z weighted by chiralities is shown in Fig. 3(a), which exhibits the anticipated A^2 increment (we have put $e = 1$). This quantity equals to the Chern vector $\delta\nu_z$ in the small A regime [Eq. (6)]. On the other hand, the resultant self-doping shows the expected A^2 dependence as illustrated in Fig. 3(b). However, it only corresponds to a higher order effect and does not affect the photoinduced AHE.

Application to TaAs family of Weyl semimetals.—TaAs was recently shown to host 24 Weyl nodes in the Brillouin zone [10,11,15]. There are two nonequivalent sets of Weyl points [10] that we denote as the P set consisting of 8 nodes at $(\pm k_x^P, \pm k_y^P, 0)$ and $(\pm k_y^P, \pm k_x^P, 0)$, and the Q set with 16 nodes at $(\pm k_x^Q, \pm k_y^Q, \pm k_z^Q)$ and $(\pm k_y^Q, \pm k_x^Q, \pm k_z^Q)$. The values of k_x^P, k_y^P, k_x^Q, k_y^Q, k_z^Q for various TaAs family of materials can be found in Ref. [10]. Applying the symmetry

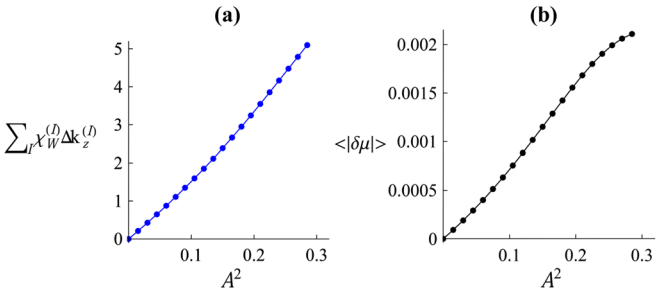

FIG. 3. The field dependence for (a) the total Δk_z weighted by chiralities and (b) the absolute self-doping $|\delta\mu|$ averaged over 12 Weyl nodes for the driven Weyl lattice model. Same parameters used as in Fig. 2.

transformation rules derived before, we find a simple rule for the node shifts for both Weyl sets:

$$\delta q_z^{(P,I)} = \chi^{(P,I)}\delta q_z^P, \quad 1 \le I \le 8,$$
$$\delta q_z^{(Q,I)} = \chi^{(Q,I)}\delta q_z^Q, \quad 1 \le I \le 16, \quad (16)$$

where $\delta q_z^{P(Q)} \propto A^2$ is the same for all 8(16) symmetry-related nodes. The z-direction momentum shift faithfully follows the chirality $\chi^{(I)}$ of each Weyl node, whereas the same is not true for the shifts in the xy plane. Therefore, the overall photoinduced AHE for the TaAs family is

$$\sigma_{xy} = \frac{e^2}{2\pi h}(8 \times \delta q^P + 16 \times \delta q^Q). \quad (17)$$

Experimental realization.—To guide future experimental efforts to observe these effects, we discuss the conditions needed and likelihood of success. In the Supplemental Material we detail our calculations of the magnitude of the Hall voltage [27], where we assume the use of a CW CO_2 laser, with a roughly constant illumination across the contacts, spaced $\approx$100 μm apart. Using established values for the Fermi velocity [13,16,20], reflectance, optical [31] and dc conductivities [18], we find a 100 nm thick film [32] of TaAs would produce a Hall signal $\approx$130 nV at room temperature, with a dc current of 1 A and 1 W laser power. We note that the small penetration depth requires the use of thinner samples to ensure most of the current is modulated by the light (the induced voltage is inversely proportional to the square of the thickness). While such signals should be straight forward to detect, even higher values may be possible through the use of pulsed lasers with higher peak electric fields, with the Hall signal detected through Faraday rotation measurements.

Conclusion.—An assortment of analyses based on Floquet theory is carried out on models of Weyl semimetals to argue that the AHE is induced generically by applying an ac electromagnetic field of a definite chirality, in the plane orthogonal to the incident beam. This photoinduced AHE originates from the remarkable monopole nature of Weyl nodes. The induced Hall conductivity scales linearly

and continuously with the field intensity. The nodal shift itself may be observable by the pump-probe ARPES, while the photoinduced AHE can be detected via dc transport or Faraday rotation experiment on films. Conceivably, the ac-field-driven AHE may exist in other materials possessing non-trivial band topology such as ferromagnetic metals [33].

P. A. L. acknowledges support from DOE Grant No. DE-FG02-03- ER46076. K. S. B. acknowledges support from the National Science Foundation under Grant No. DMR-1410846. J. H. H. is supported by the NRF grant (No. 2013R1A2A1A01006430). Y. R. is supported by the Alfred P. Sloan fellowship and National Science Foundation under Grant No. DMR-1151440.

*hanjh@skku.edu
†ying.ran@bc.edu

[1] A. H. Castro Neto, F. Guinea, N. M. R. Peres, K. S. Novoselov, and A. K. Geim, Rev. Mod. Phys. **81**, 109 (2009).
[2] M. Z. Hasan and C. L. Kane, Rev. Mod. Phys. **82**, 3045 (2010).
[3] C. Herring, Phys. Rev. **52**, 365 (1937).
[4] S. Murakami, New J. Phys. **9**, 356 (2007).
[5] X. Wan, A. M. Turner, A. Vishwanath, and S. Y. Savrasov, Phys. Rev. B **83**, 205101 (2011).
[6] K.-Y. Yang, Y.-M. Lu, and Y. Ran, Phys. Rev. B **84**, 075129 (2011).
[7] A. A. Burkov and L. Balents, Phys. Rev. Lett. **107**, 127205 (2011).
[8] Z. Fang, N. Nagaosa, K. S. Takahashi, A. Asamitsu, R. Mathieu, T. Ogasawara, H. Yamada, M. Kawasaki, Y. Tokura, and K. Terakura, Science **302**, 92 (2003).
[9] H. Nielsen and M. Ninomiya, Phys. Lett. **130B**, 389 (1983).
[10] H. Weng, C. Fang, Z. Fang, B. A. Bernevig, and X. Dai, Phys. Rev. X **5**, 011029 (2015).
[11] S.-M. Huang, S.-Y. Xu, I. Belopolski, C.-C. Lee, G. Chang, B. Wang, N. Alidoust, G. Bian, M. Neupane, C. Zhang, S. Jia, A. Bansil, H. Lin, and M. Z. Hasan, Nat. Commun. **6**, 7373 (2015).
[12] S.-Y. Xu, I. Belopolski, N. Alidoust, M. Neupane, G. Bian, C. Zhang, R. Sankar, G. Chang, Z. Yuan, C.-C. Lee, S.-M. Huang, H. Zheng, J. Ma, D. S. Sanchez, B. Wang, A. Bansil, F. Chou, P. P. Shibayev, H. Lin, S. Jia, and M. Z. Hasan, Science **349**, 613 (2015).
[13] B. Q. Lv, H. M. Weng, B. B. Fu, X. P. Wang, H. Miao, J. Ma, P. Richard, X. C. Huang, L. X. Zhao, G. F. Chen, Z. Fang, X. Dai, T. Qian, and H. Ding, Phys. Rev. X **5**, 031013 (2015).
[14] C.-C. Lee, S.-Y. Xu, S.-M. Huang, D. S. Sanchez, I. Belopolski, G. Chang, G. Bian, N. Alidoust, H. Zheng, M. Neupane, B. Wang, A. Bansil, M. Z. Hasan, and H. Lin, Phys. Rev. B **92**, 235104 (2015).
[15] B. Q. Lv, N. Xu, H. M. Weng, J. Z. Ma, P. Richard, X. C. Huang, L. X. Zhao, G. F. Chen, C. E. Matt, F. Bisti, V. N. Strocov, J. Mesot, Z. Fang, X. Dai, T. Qian, M. Shi, and H. Ding, Nat. Phys. **11**, 724 (2015).
[16] L. X. Yang, Z. K. Liu, Y. Sun, H. Peng, H. F. Yang, T. Zhang, B. Zhou, Y. Zhang, Y. F. Guo, M. Rahn, D. Prabhakaran, Z. Hussain, S.-K. Mo, C. Felser, B. Yan, and Y. L. Chen, Nat. Phys. **11**, 728 (2015).
[17] S.-Y. Xu, N. Alidoust, I. Belopolski, Z. Yuan, G. Bian, T.-R. Chang, H. Zheng, V. N. Strocov, D. S. Sanchez, G. Chang, C. Zhang, D. Mou, Y. Wu, L. Huang, C.-C. Lee, S.-M. Huang, B. Wang, A. Bansil, H.-T. Jeng, T. Neupert, A. Kaminski, H. Lin, S. Jia, and M. Zahid Hasan, Nat. Phys. **11**, 748 (2015).
[18] X. Huang, L. Zhao, Y. Long, P. Wang, D. Chen, Z. Yang, H. Liang, M. Xue, H. Weng, Z. Fang, X. Dai, and G. Chen, Phys. Rev. X **5**, 031023 (2015).
[19] C. Zhang, S.-Y. Xu, I. Belopolski, Z. Yuan, Z. Lin, B. Tong, N. Alidoust, C.-C. Lee, S.-M. Huang, H. Lin, M. Neupane, D. S. Sanchez, H. Zheng, G. Bian, J. Wang, C. Zhang, T. Neupert, M. Z. Hasan, and S. Jia, arXiv:1503.02630.
[20] C. Shekhar, A. K. Nayak, Y. Sun, M. Schmidt, M. Nicklas, I. Leermakers, U. Zeitler, Y. Skourski, J. Wosnitza, Z. Liu, Y. Chen, W. Schnelle, H. Borrmann, Y. Grin, C. Felser, and B. Yan, Nat. Phys. **11**, 645 (2015).
[21] T. Oka and H. Aoki, Phys. Rev. B **79**, 081406 (2009).
[22] Y. H. Wang, H. Steinberg, P. Jarillo-Herrero, and N. Gedik, Science **342**, 453 (2013).
[23] A. Narayan, Phys. Rev. B **91**, 205445 (2015).
[24] S. Ebihara, K. Fukushima, and T. Oka, arXiv:1509.03673.
[25] N. H. Lindner, G. Refael, and V. Galitski, Nat. Phys. **7**, 490 (2011).
[26] R. Wang, B. Wang, R. Shen, L. Sheng, and D. Y. Xing, Europhys. Lett. **105**, 17004 (2014).
[27] See Supplemental Material at http://link.aps.org/supplemental/10.1103/PhysRevLett.116.026805 for more details about the effective Weyl-Floquet Hamiltonian, the lattice model calculation, realistic experimental estimations, and the doping effect, which includes Refs. [28,29].
[28] J. H. Shirley, Phys. Rev. **138**, B979 (1965).
[29] P. Delplace, J. Li, and D. Carpentier, Europhys. Lett. **97**, 67004 (2012).
[30] T. Ojanen, Phys. Rev. B **87**, 245112 (2013).
[31] B. Xu, Y. M. Dai, L. X. Zhao, K. Wang, R. Yang, W. Zhang, J. Y. Liu, H. Xiao, G. F. Chen, A. J. Taylor, D. A. Yarotski, R. P. Prasankumar, and X. G. Qiu, arXiv:1510.00470.
[32] The proposed film has a thickness larger than the lattice spacing by 2 orders of magnitude so that the momentum along the width is still a good quantum number.
[33] N. Nagaosa, J. Sinova, S. Onoda, A. H. MacDonald, and N. P. Ong, Rev. Mod. Phys. **82**, 1539 (2010).